



Published in final edited form as:

Bone. 2006 February ; 38(2): 273–279.

Automated registration of hip and spine for longitudinal QCT studies: Integration with 3D densitometric and structural analysis

Wenjun Li^{*}, Miki Sode, Isra Saeed, and Thomas Lang

Department of Radiology, University of California at San Francisco, 185 Berry Street, Suite 350, San Francisco, CA 94143-0946, USA

Abstract

To eliminate user interaction in longitudinal quantitative computed tomography (QCT) measurements of bone mineral density (BMD) and geometry, we have developed and optimized an automated registration algorithm for QCT images of the hip and spine and integrated it with a previously developed 3D densitometric and structural analysis program. With registration, the follow-up images are automatically aligned with respect to the baseline scans, and the bone quantification of the aligned follow-up scan is initiated based on the bone morphometric features defined on the baseline scan. To validate the algorithm, we analyzed 20 pairs of repeat QCT images (10 hip pairs and 10 spine pairs) acquired on a modern multi-slice CT scanner, with repositioning between each scan pair to simulate repeat visits. Bone measurements obtained with automatic registration achieved comparable or improved precision errors compared to those obtained by careful manual analysis of the follow-up scans. The algorithm we have developed was based on the mutual information approach, with simplex optimization under a multi-resolution scheme. The average registration time was 2.3 min for a hip pair and 1.1 min for a vertebra pair using a standard desktop computer. Based on the reduced user interaction, high degree of precision, and short execution time, this is a promising technique for monitoring therapy in patients and clinical trials.

Keywords

Image registration; Mutual information; Bone mineral density; Osteoporosis; 3D quantitative computed tomography; Proximal femur; Spine

Introduction

Hip and spine fractures are the most serious manifestation of osteoporosis. For example, in the US only, they affect over 250,000 elderly and result in a 20% mortality rate and substantial loss of quality of life [4,27]. The number of hip and spine fractures is expected to increase as the population ages.

In the clinical setting, osteoporosis may be diagnosed using bone mineral density (BMD) measurements by dual X-ray absorptiometry (DXA) or by the confirmation of a fragility fracture. A positive diagnosis of osteoporosis may be followed by treatment using one of several commercially available medications, including anti-resorptive therapies [8,11] or newly approved anabolic therapies such as human recombinant parathyroid hormone (hrPTH) [18]. The use of DXA [17,23] to monitor the effect of these interventions on the hip and spine is limited by the fact that DXA measurements show changes in the total bone mass while the therapies themselves may differentially affect the cortical and trabecular compartments. Thus, using total bone mass as a surrogate marker of therapeutic efficacy may mask compartment

^{*}Corresponding author. Fax: +1 415 353 9425.E-mail address: Wenjun.Li@radiology.ucsf.edu (W. Li).

specific effects that could be important for bone strength. Quantitative computed tomography (QCT), on the other hand, permits compartment specific three-dimensional bone density and geometry assessment of the hip and spine. A recent study of postmenopausal women using QCT compared the effects of hrPTH, alendronate, and a combination of these two therapies on bone density over a year of treatment[1]. The study found that in the hip and spine, both hrPTH and alendronate increased trabecular bone density, whereas hrPTH decreased and alendronate increased cortical bone density. Interestingly, the study also reported increases in the volume of cortical bone in the subjects treated with hrPTH, but not those treated with alendronate over the year of treatment.

Computer algorithms used to analyze QCT images generally involve manual interactions [15,16,21] to define anatomic axes and, when necessary, to assist the segmentation procedure used to define the bone edges and perform the region of interest and geometric analyses. For longitudinal studies, such manual interactions introduce intra- or inter-operator precision errors, which can affect the ability of this technique to resolve small changes over the course of a therapy. Compared to highly controlled research settings, this becomes a more serious concern in clinical settings, where the user skills are highly variable. In an individual, a change may be detected with a 95% confidence level if it is 2.8 times the precision error [2,9]. Thus, precision errors should be minimized to reduce the time required to detect treatment effects.

In this study, we have developed a registration algorithm for 3D hip and spine images from commonly available QCT scanners in order to reduce precision errors related to operator variability in longitudinal QCT image analysis. The algorithm works in conjunction with a 3D analysis program [15,16] which defines regions of interest for compartmental BMD and geometric analyses of the proximal femur and vertebrae. The registration program transforms the longitudinal images and resamples them in the coordinate system of the baseline scan. The morphometric parameters, such as the orientations of the femoral neck and spinal axis defined for the baseline scan, are then used to initiate the bone segmentation and quantification process for the follow-up scan.

Our hip and spine registration algorithm is an intensity based algorithm applying the concept of mutual information [25,26], thus it eliminates the need to specify anatomic landmarks for registration. Based on a decade of experience in successful medical image registration [10, 12,29], it has become a current trend to build application-specific systems for integrating registration into routine clinical practice [3,6,7]. Because the hip and vertebrae have smaller dimensions compared to other widely studied anatomic objects in medical image registration such as the head [25,26], hip and spine images pose a greater challenge to register. Signals due to misalignments of smaller objects are of lower magnitude, with a greater tendency for the registration process to be trapped in local maxima. To this end, we have adapted optimization methods in our hip and spine registration, including using simplex searching [20] under a multi-resolution scheme [25,26], and an adaptive bin-size approach [28] with modifications.

To test the precision using our automated registration, we have applied this algorithm to 20 pairs of QCT scans, comprising 10 scan pairs of the hip and 10 pairs of the spine, obtained with a 15-min interval and repositioning between the two scans of each pair. Our goal was to determine whether the use of automated analysis could achieve comparable or better precision compared to careful manual analysis.

Materials and methods

Human subjects

20 pairs of repeat CT scans, including 10 hip pairs and 10 spine pairs, were acquired and analyzed to test the registration algorithm. The subjects were a group of postmenopausal

women. For the hip group, the mean age is 63 ± 2 years, and the t score is -1.05 ± 1.30 . For the spine group, the mean age is 64 ± 3 years, and the t score is -0.76 ± 1.69 . Each patient was scanned twice with repositioning after a time interval of 15 min between scans. Each patient provided informed consent as required by the Committee on Human Research at the University of California, San Francisco. The scanner was a Phillips MX-8000 16 detector system (Phillips Medical Systems, Eindhoven, Netherlands). CT images were calibrated to bone density using a solid hydroxyapatite calibration phantom (Image Analysis, Columbia, KY). The scanning parameter settings were 90 kVp, 280 mAs for the hip scans and 90 kVp, 140 mAs for the spine scans. Both scans used 3-mm-thick sections with a 3 mm/s table speed, with a reconstruction interval of 3 mm.

Registration algorithm

Our registration program was mutual information based, and took advantage of some specific features of the hip and spine. For QCT images, the contrast between the hip and spine cortices and the surrounding soft tissue is large, making it possible to use CT value thresholding and region-growing techniques to limit the candidate voxels for registration to bone voxels only. This can not only simplify the registration by allowing us to consider rigid body transformations only, but it also improves the registration efficiency because the number of voxels used for the alignment process is greatly reduced. The voxel dimensions in CT images are well-calibrated, permitting us to eliminate scaling operations between scans.

Prior to registration, the baseline and follow-up CT images were cropped to include only the hip or vertebrae to be registered, and the baseline scan was segmented to create a binary bone mask using a region-growing algorithm [15,16]. The registration procedure worked as follows. The input CT images were first blurred to reduce image noise, and then resampled to isotropic voxel size. The voxels from the segmented binary mask were then used to create a list of voxels to be aligned. To calculate the mutual information, we used adaptive bin sizes similar to that described in [28], where three bin sizes (16, 32, 64) were used. In our implementation, however, we allowed the bin size to be variable such that the average number of voxels in each bin was 40, under the restriction that the minimum number of bins was not less than 16.

At each registration step, based on the current configuration of the baseline and follow-up images, a normalized mutual information [24] was calculated from the voxels in these bins. The program then iteratively searched for the optimal transformation in the 6-D parameter space (3 translations and 3 rotations) using simplex optimization [20]. To speed up the registration and to avoid local maxima at the startup, we also applied a 3-level multi-resolution scheme [10,26], with resampling sizes of 1.5 mm, 1.0 mm, and 0.75 mm.

In longitudinal measurements of hip and spine, when bone changes exist, the internal trabecular bone usually changes more than the outer cortical bone. To take this into account, we further limited the voxels used for registration to the outer cortical boundary voxels only, defining a small window near the proximal femoral or vertebral boundary that encompassed the outer cortex and a thin ribbon of surrounding soft tissue. The boundary was automatically defined based on the binary mask segmented from the baseline images.

Evaluation of registration and bone measurements

To validate the registration program, we applied it to 10 hip and 10 spine pairs of repeat scans, and examined the alignment using visual inspection as well as the reproducibility of the quantitative bone parameters.

Visual inspection

First, the registered images were visually inspected. To qualitatively assess the degree of alignment, we drew the contour of the outer boundary of the baseline femur or vertebra, and then projected it onto the registered follow-up images. To further assess possible misalignments, we also calculated the difference images by subtracting the aligned follow-up images from the baseline images.

Bone parameter quantification

Upon completion of registration, the registered follow-up images were automatically processed for segmentation and definition of the regions of interest (ROIs) based on the morphometric features identified and defined in the baseline analysis. Note that instead of simply superposing the ROIs defined from the baseline onto the follow-up scan, we allowed the aligned follow-up images to be re-segmented and the ROIs redefined. This allowed the program to take into account possible periosteal apposition effects thought to be associated with aging and anabolic drug therapies [19,22]. After the ROIs were defined, quantification of femoral and spinal parameters was subsequently performed using an algorithm previously described in [15,16], which determined the cortical, trabecular, and integral bone mineral density, volume, and mineral content values. For the hip, the ROIs included regions encompassing the entire proximal part of the femur, the femoral neck, and a region encompassing both trochanters. In addition to the BMD measures, we also computed several geometric parameters, including the total tissue volumes within the periosteal boundaries of the femoral neck, trochanteric and total femur regions of interest, and the minimum and maximum cross-sectional areas of tissue within the periosteal boundaries of the total femur region of interest (CSA_{min} and CSA_{max}).

For the hip, we calculated the moments of inertia, I_x and I_y , in the body-fixed x and y axes at the location of the femoral neck slice of minimum tissue cross-sectional area (CSA_{min}). These were used to derive the femoral neck bending strength index (fnBSI) [14]

$$fnBSI = \frac{I_x + I_y}{2\sqrt{\frac{CSA_{min}}{\pi}}}$$

Spinal analyses involved the lumbar vertebrae L1 and L2. Since they are not rigidly connected to each other, the registration and quantification were performed separately for L1 and L2, with the same set of vertebral parameters calculated after each registration. The vertebral ROIs were those described in [16]. Integral and trabecular ROIs were determined both on a 10-mm-thick section through the mid-vertebra and on the entire vertebra, and a cortical region was defined around the cortex of the entire vertebra. For both the mid-plane and total vertebra, the integral regions included a region encompassing only the vertebral centrum and another region encompassing the centrum and posterior elements. Additionally, we also derived from the CT images a simulated DXA BMD. Geometric bone parameters included the length of vertebral body between the anterior aspect of the cortex and the anterior aspect of the spinal canal, and the lateral width of the vertebral body at the level of anterior spinal canal. Additionally, the vertebral cross-sectional area was quantified. We also calculated the vertebral compressive strength index [14] as

$$CSI = BMD_{mv}^2 \times CSA_{mv}$$

where BMD_{mv} and CSA_{mv} are the integral BMD and cross-sectional area of the mid-vertebral section.

After registration of each pair, the difference between each quantified BMD or geometric bone parameter for the baseline and follow-up scans was calculated. To avoid the bias in calculating a percentage difference, we used the coefficient of variation:

$$CV = \frac{\sqrt{(v^b - v)^2 + (v^f - v)^2}}{v} \times 100$$

where v^b was the bone parameter quantified from the baseline-scan, and v^f was the corresponding value from the registered follow-up scan, and v was the average. Ideally, since there was no bone change for a repeat scan pair, the CV value would become zero with a perfect alignment. Thus, its non-vanishing value served as an indication of the degree of misalignment.

To calculate the precision for each BMD and geometric measurement, we used the precision definition given by Gluer et al. [9], which was the root-mean-square of the CVs calculated from the scan pairs

$$\text{precision} = \sqrt{\frac{\sum_{i=1}^N CV_i^2}{N}}$$

Results

Visual inspection of registered images

An example of the aligned baseline and follow-up images is displayed in Fig. 1. Fig. 1 compares the matched proximal femoral cross-sections from the baseline and the aligned follow-up images, as well as the difference images from the corresponding cross-sections. Fig. 1 has the first set of three images in coronal view, and the following three sets in axial view. For each set, the boundary was drawn on the baseline image and directly superimposed on the follow-up image, showing good qualitative agreement with the bone edge on the follow-up image. The internal structures in the scans were also well reproduced. The alignment can also be seen from the difference images, where the registered part (the proximal femur) showed close to vanishing intensities, while the un-registered structures outside the proximal femur had high remaining intensities.

Precision of BMD and geometric measurements obtained using manual and automated methods

We show in Table 1 and Table 2 the precision errors for the quantified bone parameters in the proximal femur and spine using automated registration, and compare them to the manual results.

Hip

Table 1 shows the measurement results of the hip parameters. The first numerical column shows the average values for these parameters and their standard deviations, followed by the measured differences (errors) between the baseline and follow-up scans as calculated by the root-mean-square (RMS) values from the 10 pairs in physical units, with and without registration.

The measurement precision errors and the CV deviations are also shown in Table 1. For BMD measurements with registration, Table 1 shows that the precision errors for total femur and trochanter varied from 0.60% (trochanteric trabecular BMD) to 1.42% (trochanteric cortical BMD). Neck BMD precision errors were relatively larger because of the smaller volume of bone assessed, and because the fatty infiltration of the medullary cavity in the femur produced low trabecular BMD and thus high CV values. It also shows that by using automated registration, most of the individual BMD precision errors were smaller than those obtained by manual analysis of the follow-up scans.

Compared to BMD, the geometric parameters generally showed larger precision errors. As can be seen from Table 1, for the volume measurements of neck, trochanter, and total femur, the precision errors varied from 2.21% to 3.65%. But we can still see that for all the individual volume parameters, the precision errors were relatively smaller than those obtained by manual analysis. Registration gave a precision error for the minimum cross-sectional area (CSA_{\min}) of 1.51%, which was slightly larger than that obtained by manual results of 1.44%. However, for the maximum cross-sectional area (CSA_{\max}), registration showed a significant decrease of precision error. For the femoral neck bending strength index (fnBSI), the registration gave a precision error of 3.66%, compared to 5.09% obtained by manual analysis.

Based on the CV values of the 10 hip pairs, we performed t tests and F tests to determine whether the registration process reduced the mean values and the standard deviations of the CVs, respectively. The improvement in measurements showed statistical significance for some of the bone parameters, as marked by signs of * (*t* test with a P value less than 0.05) or † (*F* test with a P value less than 0.05) in Table 1. For example, for trochanter trabecular BMD, a t test gave a P value of 0.021. For CSA_{\max} , the P value was 0.017. For the F test, the P value was 0.031 for Neck cortical BMD, and 0.00002 for CSA_{\max} .

Spine

For each spine pair, two vertebrae, L1 and L2 were registered individually, and the same set of bone parameters were calculated. The measurements are shown in Table 2, where for each bone parameter, the results from L1 and L2 were also treated individually. By using registration, the precision errors of trabecular and integral bone BMD values varied from 0.90% to 1.99%, which were generally smaller than those obtained by manual analysis. For all the three geometric parameters and the derived mechanical parameter (compressive strength index), registration showed decreased precision errors. Additionally, we also calculated a simulated DXA areal BMD, which showed a precision error of 1.84% by using registration, compared to 3.10% by using manual analysis.

The improvement in precision errors and the deviations of errors were observed with statistical significance for some of the spine parameters, as marked by signs of * (*t* test) or † (*F* test). For example, a t test for the DXA simulated areal BMD showed a P value of 0.026, and F tests showed P values of 0.00003 (3D trabecular BMD), 0.033 (3D total integral BMD), 0.0016 (3D centrum integral BMD), and 0.0027 (vertebral cross-sectional area).

CPU time for registration

The average CPU time executing each registration was 138 s for a hip pair, and 69 s for a single vertebra pair. We used a Dell workstation with a Pentium 4 processor, 2.4 GHz CPU and 1.5 Gb RAM.

Discussion

Longitudinal bone measurements of the hip and spine, as demonstrated by our registration algorithm, can be automated to reduce user interaction. Based on the 20 pairs of repeat scans with repositioning, the precision errors for BMD and geometric measurements were generally improved or were comparable to those obtained by manual analysis of the follow-up scans.

Reduction of user interaction can greatly affect the application of the QCT imaging technique for longitudinal measurements, especially in cases where there is substantial turnover in technical personnel and high variability in operator skill and training. Our approach for automated registration of volumetric images reduces user interaction both in the acquisition, because the 3D image obviates the need for careful selection of a transverse section, and in analysis because the image analyst does not have to place landmarks on the serial images.

Compared to DXA, which provides a purely integral bone measurement, QCT has the advantage of measuring bone compartments individually. According to the recent report from a 1 year trial of 238 postmenopausal women undergoing treatment with hrPTH, alendronate, and their combination [1], the change in trabecular BMD over a year was 2-3 fold larger than that of the integral bone envelope. By detecting such compartment specific changes with QCT imaging, we expect that the time required to determine the efficacy of an intervention such as alendronate or hrPTH could be greatly shortened.

We selected the approaches reported here among other registration algorithms based on several reasons. First, at each registration step, to select a figure of merit, i.e., the measure of the “goodness” of the alignment between the baseline and follow-up images, direct comparison of the CT values between scans is easily implemented and could be a choice. However, this may not be valid when the scanning settings differ between the baseline and the follow-up scans. Mutual information, on the other hand, is less affected by such factors because it is calculated based on the image intensity distribution statistics associated with the physical bone structures. Secondly, for 3D medical image registration, avoidance of local maxima is an important concern, particularly for small objects such as the hip and spine. Optimization methods such as hill-climbing, have been demonstrated to be effective for registering head scans[25,26]. However, for the hip and spine, we found the simplex method to be more robust.

Besides improving the precision of BMD measurements, the degree of alignment obtained using our methodology facilitates studies of the regional changes of bone geometric and mechanical properties, such as cross-sectional areas and moments of inertia. Because moments of inertia involve sums of cortical intensities weighted by distance from the neutral axis, they are highly subject to repositioning errors in the tissue sections being evaluated. Another potential application of our approach is for finite element modeling [5,13], where consistent loading conditions must be applied to serial scans. By aligning such scans automatically, it may be possible to use the identical loading conditions in serial images.

In addition to these strengths, however, this study also has limitations. Although we have seen that using automated registration generally gave improved precision, the improvement was not statistically significant for most bone parameters because of small sample size. Another reason for this may also be that the manual results reported here were obtained in a research setting, and conducted by an experienced image analyst operating under well-controlled quality assurance processes. Such factors may or may not be available in the general clinical setting. Secondly, we should note that compared to manual analysis, registration inevitably involves an additional transformation to align the follow-up scan to the baseline scan. The image interpolation associated with this introduces partial volume averaging, which could affect thin structures such as the femoral neck and vertebral cortices, resulting in precision errors for some variables that may be comparable to or slightly larger than the corresponding manual values. In general, as shown in Tables 1 and 2, compared to the relatively more unpredictable errors arising from operator interaction, the errors resulting from this alignment transformation were relatively small. These may be further reduced in future implementations involving more sophisticated interpolation schemes or higher resolution scanning protocols.

In summary, we have developed and optimized a registration algorithm for hip and spine QCT images that automates longitudinal bone measurements and reduces user interaction. Based on 20 pairs of repeat scans with repositioning, the registration algorithm has shown precision errors which are generally smaller than those obtained by manual analysis. By reducing user interaction, the resulting reduction in the magnitude and variability of precision errors should increase the applicability of this technique in the clinical setting. If prospectively designed, trials show that QCT measurements predict changes in fracture incidence comparably or better

than DXA measurements, their high precision and responsiveness may result in a more effective and widely accepted technique for monitoring therapy in osteoporosis.

Acknowledgments

This research was supported by grants NIH-R42-AR45713-R1A2. The authors are grateful for the assistance of Vesta March CRT for image acquisition. The authors also thank Sharmila Majumdar, Sven Prevrhal, Ying Lu, and Margarita Meta for helpful discussions.

References

1. Black DM, Greenspan SL, Ensrud KE, Palermo L, McGowan JA, Lang TF, et al. The effects of parathyroid hormone and alendronate alone or in combination in postmenopausal osteoporosis. *N Engl J Med* 2003;349(13):1207–15. [PubMed: 14500804]
2. Bonnicksen SL, Johnston J Jr, Kleerekoper M, Lindsay R, Miller P, Sherwood L, et al. Importance of precision in bone density measurements. *J Clin Densitom* 2001;4(2):105–10. [PubMed: 11477303]
3. Chen CT. Radiologic image registration: old skills and new tools. *Acad Radiol* 2003;10(3):239–41. [PubMed: 12643549]
4. Chrischilles E, Shireman T, Wallace R. Costs and health effects of osteoporotic fractures. *Bone* 1994;15(4):377–86. [PubMed: 7917575]
5. Cody DD, Gross GJ, Hou FJ, Spencer HJ, Goldstein SA, Fyhrie DP. Femoral strength is better predicted by finite element models than QCT and DXA. *J Biomech* 1999;32(10):1013–20. [PubMed: 10476839]
6. Cohade C, Osman M, Leal J, Wahl RL. Direct comparison of (18)F-FDG PET and PET/CT in patients with colorectal carcinoma. *J Nucl Med* 2003;44(11):1797–803. [PubMed: 14602862]
7. Court LE, Dong L. Automatic registration of the prostate for computed-tomography-guided radiotherapy. *Med Phys* 2003;30(10):2750–7. [PubMed: 14596313]
8. Cummings SR, Karf DB, Harris F, Genant HK, Ensrud K, LaCroix AZ, et al. Improvement in spine bone density and reduction in risk of vertebral fractures during treatment with antiresorptive drugs. *Am J Med* 2002;112(4):281–9. [PubMed: 11893367]
9. Glüer CC, Blake G, Blunt BA, Jergas M, Genant HK. Accurate assessment of precision errors: how to measure the reproducibility of bone densitometry techniques. *Osteoporosis Int* 1995;5(5):262–70.
10. Hill DL, Batchelor PG, Holden M, Hawkes DJ. Medical image registration. *Phys Med Biol* 2001;46(3):R1–45. [PubMed: 11277237]
11. Hosking D, Chilvers CE, Christiansen C, Ravn P, Wasnich R, Ross P, et al. Prevention of bone loss with alendronate in postmenopausal women under 60 years of age. Early Postmenopausal Intervention Cohort Study Group. *N Engl J Med* 1998;338(8):485–92. [PubMed: 9443925]
12. Hutton BF, Braun M. Software for image registration: algorithms, accuracy, efficacy. *Semin Nucl Med* 2003;33(3):180–92. [PubMed: 12931320]
13. Keyak J. Improved prediction of proximal femoral fracture load using nonlinear finite element models. *Med Eng Phys* 2001;23(3):165–73. [PubMed: 11410381]
14. Lang T, LeBlanc A, Evans H, Lu Y, Genant H, Yu A. Cortical and trabecular bone mineral loss from the spine and hip in long-duration spaceflight. *J Bone Miner Res* 2004;19(6):1006–12. [PubMed: 15125798]
15. Lang TF, Keyak JH, Heitz MW, Augat P, Lu Y, Mathur A, et al. Volumetric quantitative computed tomography of the proximal femur: precision and relation to bone strength. *Bone* 1997;21(1):101–8. [PubMed: 9213015]
15. Lang TF, Li J, Harris ST, Genant HK. Assessment of vertebral bone mineral density using volumetric quantitative CT. *J Comput Assist Tomogr* 1999;23(1):130–7. [PubMed: 10050823]
17. Mazess RB, Collick B, Trempe J, Barden H, Hanson J. Performance evaluation of a dual energy X-ray bone densitometer. *Calcif Tissue Int* 1989;44:228–32. [PubMed: 2493329]
18. Neer RM, Arnaud CD, Zanchetta JR, Prince R, Gaich GA, Reginster JY, et al. Effect of parathyroid hormone (1-34) on fractures and bone mineral density in postmenopausal women with osteoporosis. *N Engl J Med* 2001;344(19):1434–41. [PubMed: 11346808]

19. Oxlund H, Ejersted C, Andreassen TT, Topping O, Nilsson MH. Parathyroid hormone (1-34) and (1-84) stimulate cortical bone formation both from periosteum and endosteum. *Calcif Tissue Int* 1993;53(6):394-9. [PubMed: 8293353]
20. Press, WH.; Teukolsky, SA.; Vetterling, WT.; Flannery, BP. Numerical recipes. Cambridge Univ. Press; C. Cambridge, UK: 1999. p. 394-455.
21. Pevrhal S, Fox JC, Shepherd JA, Genant HK. Accuracy of CT-based thickness measurement of thin structures: modeling of limited spatial resolution in all three dimensions. *Med Phys* 2003;30(1):1-8. [PubMed: 12557971]
22. Riggs BL, Melton III LJ, Robb RA, Camp JJ, Atkinson EJ, Peterson JM, et al. Population-based study of age and sex differences in bone volumetric density, size, geometry, and structure at different skeletal sites. *Bone Miner Res* 2004;19(12):1945-54.
23. Stein JA, Lazewatsky JL, Hochberg AM. Dual energy X-ray bone densitometer incorporating an internal reference system. *Radiology* 1987;165(P):313. [PubMed: 3310091]
24. Studholme C, Hill DL, Hawkes DJ. An overlap invariant entropy measure of 3D medical image alignment. *Pattern Recogn* 1999;32(1):71-86.
25. Studholme C, Hill DL, Hawkes DJ. Automated 3-D registration of MR and CT images of the head. *Med Image Anal* 1996;1(2):163-75. [PubMed: 9873927]
26. Studholme C, Hill DL, Hawkes DJ. Automated three-dimensional registration of magnetic resonance and positron emission tomography brain images by multiresolution optimization of voxel similarity measures. *Med Phys* 1997;24(1):25-35. [PubMed: 9029539]
27. Woolf AD, Pflieger B. Burden of major musculoskeletal conditions. *Bull World Health Organ* 2003;81(9):646-56. [PubMed: 14710506]
28. Zhu YM, Cochoff SM. Influence of implementation parameters on registration of MR and SPECT brain images by maximization of mutual information. *J Nucl Med* 2002;43(2):160-6. [PubMed: 11850479]
29. Zitová B, Flusser J. Image registration methods: a survey. *Image Vis Comput* 2003;21(11):977-1000.

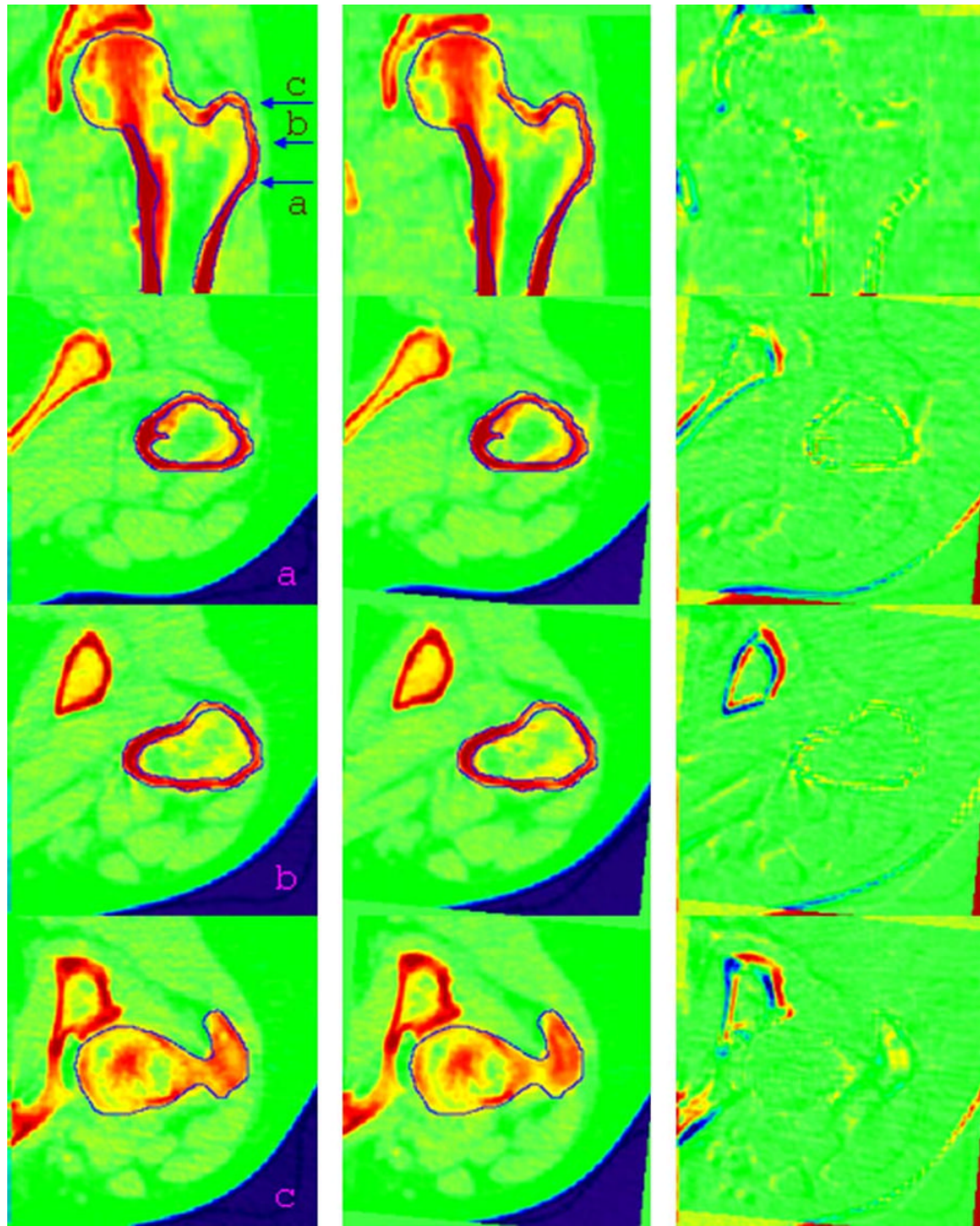


Fig. 1. Coronal and axial cross-sections from the baseline (left), the aligned follow-up (middle) and the difference images (right) of a hip repeat scan pair. The arrows with labels in the coronal cross-section of the baseline scan indicate the positions from which the following axial views are taken. The femur boundaries outlined from the baseline images are superimposed onto the follow-up images to check their alignment. The registered part (proximal femur) shows vanishing intensities in the difference images. For better illustration, false colors were applied to the CT values.

Table 1
Comparison of hip measurements obtained from 10 scan pairs using manual analysis and automated registration

	Measurement in physical units		CV (%)	
	Average value \pm standard Deviation	Error _{registration} (error _{manual})	Precision _{registration} (precision _{manual})	Deviation _{registration} (deviation _{manual})
Neck integral BMD (g/cm ³)	0.273 \pm 0.039	0.005 (0.005)	1.31 (1.56)	0.80 (1.17)
Neck trabecular BMD (g/cm ³)	0.089 \pm 0.032	0.005 (0.006)	4.53 (5.85)	2.74 (3.21)
Neck cortical BMD (†) (g/cm ³)	0.521 \pm 0.030	0.012 (0.022)	1.61 (2.89)	1.06 (2.30)
Troch integral BMD (g/cm ³)	0.262 \pm 0.038	0.003 (0.005)	0.81 (1.31)	0.59 (0.81)
Troch trabecular BMD (*)(g/cm ³)	0.111 \pm 0.035	0.001 (0.002)	0.60 (1.20)	0.43 (0.78)
Troch cortical BMD (g/cm ³)	0.526 \pm 0.035	0.011 (0.011)	1.42 (1.49)	0.81 (0.73)
Total femur integral BMD (g/cm ³)	0.262 \pm 0.036	0.004 (0.004)	0.87 (1.14)	0.67 (0.59)
Total femur trabecular BMD (g/cm ³)	0.109 \pm 0.033	0.001 (0.001)	0.82 (0.72)	0.63 (0.30)
Total femur cortical BMD (g/cm ³)	0.511 \pm 0.030	0.009 (0.010)	1.24 (1.36)	0.86 (0.69)
Neck integral vol. (cm ³)	16.594 \pm 2.666	0.719 (0.933)	3.65 (3.85)	2.41 (1.74)
Neck cortical vol. (cm ³)	6.850 \pm 1.338	0.276 (0.454)	3.07 (4.28)	1.93 (2.49)
Troch integral vol. (cm ³)	76.401 \pm 12.332	3.118 (3.947)	2.80 (3.79)	1.60 (2.13)
Troch cortical vol. (cm ³)	26.038 \pm 5.277	1.154 (1.629)	2.80 (4.14)	1.58 (2.26)
Total femur integral vol. (cm ³)	99.241 \pm 15.721	3.311 (3.979)	2.54 (2.74)	1.77 (1.52)
Total femur cortical vol. (cm ³)	35.622 \pm 6.906	1.177 (1.905)	2.21 (3.37)	1.45 (1.98)
CSA _{min} (cm ²)	10.715 \pm 0.815	0.233 (0.226)	1.51 (1.44)	0.93 (0.87)
CSA _{max} (* †) (cm ²)	29.049 \pm 2.947	0.202 (0.854)	0.48 (2.18)	0.23 (1.34)
fnBSI (cm ³)	0.530 \pm 0.082	0.025 (0.037)	3.66 (5.09)	2.08 (3.07)

The first numerical column shows the average values for bone mineral density (BMD) and geometric parameters, along with their standard deviations. They are followed by the root-mean-square (RMS) errors between the baseline and follow-up scans in physical units. Precision is calculated as the RMS of the coefficients of variation (CVs) of the 10 pairs, with the CV deviations shown at right. A mark * or † after the name of a bone parameter indicates registration reduced the mean value (*) or deviation (†) of the CVs with statistical significance (*P* value less than 0.05).

Table 2

Comparison of spine measurements obtained from 10 scan pairs using manual analysis and automated registration

	Measurement in physical units		CV (%)	
	Average value ± standard deviation	Error _{registration} (error _{manual})	Precision _{registration} (precision _{manual})	Deviation _{registration} (deviation _{manual})
Mid-vert. trabecular BMD (g/ cm ³)	0.132 ± 0.034	0.003 (0.005)	1.99 (2.93)	1.13 (2.93)
Mid-vert. total integral BMD (g/ cm ³)	0.227 ± 0.036	0.005 (0.006)	1.76 (1.76)	1.07 (1.09)
Mid-vert. centrum integral BMD (g/ cm ³)	0.158 ± 0.031	0.004 (0.004)	1.75 (2.01)	1.19 (1.41)
3D trabecular BMD (†) (g/ cm ³)	0.143 ± 0.037	0.004 (0.007)	1.92 (3.56)	0.94 (2.65)
3D total integral BMD (†) (g/ cm ³)	0.224 ± 0.033	0.003 (0.004)	0.90 (1.19)	0.51 (0.85)
3D centrum integral BMD (†) (g/ cm ³)	0.176 ± 0.030	0.003 (0.004)	0.98 (1.42)	0.48 (1.03)
3D cortical BMD (g/ cm ³)	0.190 ± 0.022	0.006 (0.006)	2.11 (1.89)	1.00 (1.26)
Simulated DXA BMD (°) (g/cm ²)	0.959 ± 0.227	0.023 (0.043)	1.84 (3.10)	1.35 (1.89)
Vertebral AP length (mm)	39.350 ± 3.175	0.671 (0.775)	1.25 (1.40)	0.96 (0.91)
Vertebral lateral width (mm)	43.800 ± 3.784	0.742 (1.449)	1.15 (2.18)	0.93 (1.84)
Cross- sectional area (†) (cm ²)	9.774 ± 1.603	0.217 (0.383)	1.61 (2.41)	0.87 (1.79)
Compressive strength index (g ² / cm ⁴)	0.253 ± 0.113	0.012 (0.017)	3.31 (5.33)	2.29 (3.36)

The first numerical column shows the average values for bone mineral density (BMD) and geometric parameters, along with their standard deviations. They are followed by the root-mean-square (RMS) errors between the baseline and follow-up scans in physical units. Precision is calculated as the RMS of the coefficients of variation (CVs) of the 10 pairs, with the CV deviations shown at right. A mark * or ° after the name of a bone parameter indicates registration reduced the mean value (*) or deviation (°) of the CVs with statistical significance (P value less than 0.05).